

# Cavity QED Photons for Quantum Information Processing

Motab M. Alqahtani,<sup>1</sup> Mark S. Everitt,<sup>2</sup> and Barry M. Garraway<sup>1</sup>

<sup>1</sup>*Department of Physics and Astronomy, University of Sussex, Falmer, Brighton, BN1 9QH, United Kingdom*

<sup>2</sup>*National Institute of Informatics, 2-1-2 Hitotsubashi, Chiyoda-ku, Tokyo 101-8430, Japan*

(Dated: September 13, 2018)

Based on a multimode multilevel Jaynes-Cummings model and multiphoton resonance theory, a set of universal two- and three-qubit gates, namely the iSWAP and the Fredkin gates, has been realized where dual-rail qubits are encoded in cavities. In this way the information has been stored in cavities and the off-resonant atomic levels have been eliminated by the semi-classical theory of an effective two-level Hamiltonian. A further semi-classical model, namely the spin- $J$  model, has been introduced so that a complete population inversion for levels of interest has been achieved and periodic multilevel multiphoton models have been performed. The combination of the two semi-classical models has been employed to address two-level, three-level, four-level, and even five-level configurations. The impact of decoherence processes on the fidelity of the iSWAP and the Fredkin gates has been studied.

PACS numbers: 42.50.Pq, 42.50.Ex, 03.67.Lx

## I. PHOTONIC LOGIC

Photonic systems are an attractive choice for quantum information processing because photons form a natural interface with optical telecommunications and existing telecoms technology. However, making this choice raises a number of issues which have to be addressed. It becomes important to be able to generate single photons, a challenge, but there are now various schemes available [1–3]. A key issue, however, concerns how to process single photons as qubits and this is the issue addressed in this paper along with the fact that single photons are very *fragile*. On the other hand some aspects of photonic computation are very straightforward. For example the wires of quantum circuits can be represented by optical paths and the delay of a photonic qubit is a simple way of achieving changes of phase.

In the following we will use the optical language of photons but in the discussion of the experimental realisation of the models of this work note that we will also consider microwave photons.

A simple way to realise photonic qubits would be if the presence of a photon signifies a state  $|1\rangle$  and the absence of the photon indicates the state  $|0\rangle$ . To achieve an entangling quantum gate we could try to arrange for these qubits to interact through the action of a beam-splitter:

$$\begin{aligned} |00\rangle &\longrightarrow |00\rangle \\ |01\rangle &\longrightarrow \frac{1}{\sqrt{2}}(|01\rangle + i|10\rangle) \\ |10\rangle &\longrightarrow \frac{1}{\sqrt{2}}(|10\rangle + i|01\rangle) \\ |11\rangle &\longrightarrow \frac{1}{\sqrt{2}}(|20\rangle + |02\rangle). \end{aligned} \quad (1)$$

However, this unfortunately produces states like  $|20\rangle$  which are not qubit encodings in the original simple scheme. An alternative approach would be to try a non-

linear cross-Kerr interaction [4, 5] where

$$H_x = \chi_x \hat{a}_1^\dagger \hat{a}_1 \hat{a}_2^\dagger \hat{a}_2.$$

Then the time evolution  $\exp(-iH_x t/\hbar)$ , acting on  $|00\rangle, |01\rangle$  and  $|10\rangle$ , results in no change to the state, and the input state  $|11\rangle$  is modified by a phase factor  $\exp(-i\chi_x t/\hbar)$ . If  $\chi_x t/\hbar = \pi$ , the CZ gate (controlled- $Z$  gate), could be realised where:

$$\begin{aligned} |00\rangle &\longrightarrow |00\rangle \\ |01\rangle &\longrightarrow |01\rangle \\ |10\rangle &\longrightarrow |10\rangle \\ |11\rangle &\longrightarrow -|11\rangle. \end{aligned} \quad (2)$$

This can be represented by the table

$$\text{CZ} \equiv \begin{bmatrix} 1 & & & \\ & 1 & & \\ & & 1 & \\ & & & -1 \end{bmatrix}. \quad (3)$$

Here, and in the following we will assume that such tables are expressed in the standard qubit basis  $\{|00\rangle, |01\rangle, |10\rangle, |11\rangle\}$ . The CZ-gate is a universal quantum gate when combined with single qubit rotations. However, for the Hamiltonian  $H_x = \chi_x \hat{a}_1^\dagger \hat{a}_1 \hat{a}_2^\dagger \hat{a}_2$  the non-linearity is too weak to achieve this simple gate in this way [6, 7].

In the linear optical quantum computing vision [8] non-linear optics can be avoided in qubit processing by including photon detection in the computation process. Measurement projection is an interruptive and hence non-linear process which can be configured for quantum information processing and which includes heralding to indicate the successful arrival of photons through the processor. In achieving this the KLM scheme (Knill, Laflamme, Milburn [9]) was a breakthrough. Here the undesirable output states  $|02\rangle$  and  $|20\rangle$  are avoided by the use of a special non-linear sign gate indicated by NLS. The NLS

gate has the special property that for the general input state  $\alpha|0\rangle + \beta|1\rangle + \gamma|2\rangle \rightarrow \alpha|0\rangle + \beta|1\rangle - \gamma|2\rangle$  so that there is a sign change for the amplitude of the  $|2\rangle$  state. This means that this gate has no effect on the three basic input states  $\{|00\rangle, |01\rangle, |10\rangle\}$  which work well with a beam-splitter, and thus the gate acts as a Mach-Zehnder interferometer. For the  $|11\rangle$  input, however, the change of sign from the NLS components ensures that the output is a sign flipped  $|11\rangle$  state. However, the NLS gate has a maximum theoretical probability of  $1/4$  for success [10]. This can start to be an issue if very large numbers of gate operations are required.

For these reasons we will move away from flying photonic qubits in the following and examine the possibilities for stationary photonic qubits in a cavity. The advantage is that we already know we can realise an extremely strong non-linear interaction between photonic qubits, i.e. through a multimode Jaynes-Cummings model (JCM). We already know in the case of the single-mode JCM that the interaction can be so strong that the system exhibits Rabi oscillations [11]. However, a critical issue to examine is the decay of the system, both through cavity decay and through atomic decay (cavity modified spontaneous emission).

In the following we consider some multimode, multi- $\Lambda$  cavity QED systems for quantum information processing. We start with a simple two-mode, single  $\Lambda$  system in section II. After examining this system's weaknesses we introduce a four-mode double- $\Lambda$  system in section III. Section IV examines the dynamics of the four mode resonance with and without intermediate resonant states: intermediate resonant states can achieve a speed-up. This study includes an examination of decoherence effects. Section V examines some three-qubit gates and single qubit rotations. The paper concludes in section VI and several Appendices follow with details of some of the calculations of effective Hamiltonians for these multi-state, multimode systems.

## II. A TWO-MODE $\Lambda$ -SYSTEM

In Ref. [12], a system involving two EM modes interacting with a three level atomic  $\Lambda$ -system (see Fig. 1) has been examined. The Hamiltonian for this system, in the Rotating Wave Approximation (RWA), is then given by

$$H_I = -\Delta_b \hat{n}_1 + g_1^{\text{cb}} \left( \hat{a}_1 \hat{\sigma}_{bc} + \hat{a}_1^\dagger \hat{\sigma}_{cb} \right) - \Delta_a \hat{n}_2 + g_2^{\text{ac}} \left( \hat{a}_2 \hat{\sigma}_{ac} + \hat{a}_2^\dagger \hat{\sigma}_{ca} \right), \quad (4)$$

where  $\hat{a}_1$  and  $\hat{a}_2$  are the boson operators for the two modes, the atomic operators have the form  $\sigma_{\mu\nu} \equiv |\mu\rangle\langle\nu|$ , and  $g_{1,2}$  are the atom-field coupling constants. The definitions of the system detunings are  $\Delta_a = (\omega_c - \omega_a) - \omega_2$  and  $\Delta_b = (\omega_c - \omega_b) - \omega_1$ .

We can consider the limit for a two-photon process when the detuning  $\Delta_a = \Delta_b \rightarrow \Delta$ . In this limit we can

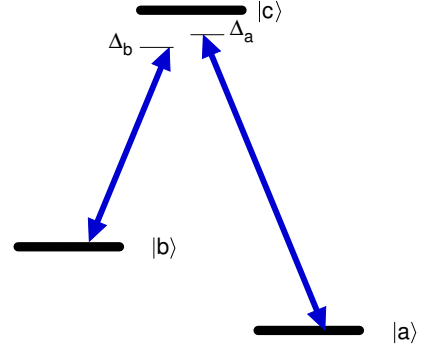


FIG. 1. A three-level atom in  $\Lambda$ -configuration, with lower levels  $|a\rangle$ ,  $|b\rangle$  and upper level  $|c\rangle$ , interacts with two cavity modes  $\omega_1$  and  $\omega_2$ . The states  $|b\rangle$  and  $|a\rangle$  couple to  $|c\rangle$  through a dipole interaction with modes one and two respectively.

perform a standard adiabatic elimination [13] to realise an effective Hamiltonian

$$H = g(\hat{a}_2^\dagger \hat{a}_1 \hat{\sigma}^- + \hat{a}_2 \hat{a}_1^\dagger \hat{\sigma}^+), \quad (5)$$

where we have introduced operators that effectively make direct transitions between the two ground states, i.e.  $\hat{\sigma}^+ = |b\rangle\langle a|$ ,  $\hat{\sigma}^- = |a\rangle\langle b|$ . The adiabatic elimination results in an effective coupling

$$g = g_{ac}g_{bc}/\Delta. \quad (6)$$

This system makes transitions between the two ground states if it is possible to extract a photon from one of the modes and transfer it to the other one. We can quickly find a general solution to the Hamiltonian (5) which is reminiscent of the Jaynes-Cummings model itself, but with two-index terms in the Rabi frequency because of the two modes [12]:

$$|\Psi(t)\rangle \simeq \sum_{n,m} C_n^{(1)} C_m^{(2)} \left\{ c_a \left[ \cos(gt\sqrt{(n+1)m})|n, m, a\rangle - i \sin(gt\sqrt{(n+1)m})|n+1, m-1, b\rangle \right] + c_b \left[ \cos(gt\sqrt{(m+1)n})|n, m, b\rangle - i \sin(gt\sqrt{(m+1)n})|n-1, m+1, a\rangle \right] \right\}.$$

We have considered the potential for logic operations, but note that for some obvious input states we have mappings where state  $|1, 1, a\rangle \rightarrow |1, 1, a\rangle, |2, 0, b\rangle$  at frequency  $g\sqrt{2}$ , and state  $|0, 1, a\rangle \rightarrow |0, 1, a\rangle, |1, 0, b\rangle$  at frequency  $g$ . These frequencies are non-commensurate which makes it awkward to eliminate  $|2, 0\rangle$  and obtain a standard gate. However, for higher photon numbers the state  $|3, 3, a\rangle \rightarrow |3, 3, a\rangle, |4, 2, b\rangle$  at frequency  $2g\sqrt{3}$  and the state  $|0, 3, a\rangle \rightarrow |0, 3, a\rangle, |1, 4, b\rangle$  at frequency  $g\sqrt{3}$ , which are commensurate frequencies. Thus, when  $gt\sqrt{3} = \pi$

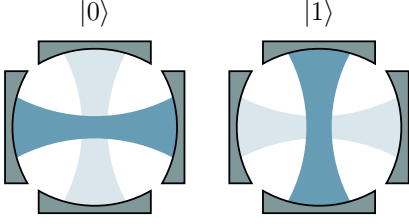


FIG. 2. Schematic showing the relationship of logical qubits to cavity mode excitations (indicated as a darker colour). The case of two cavity modes is illustrated.

the atom becomes an ancilla and

$$\begin{aligned}
 |0, 0, a\rangle &\rightarrow |0, 0, a\rangle & |0, 0, b\rangle &\rightarrow |0, 0, b\rangle \\
 |0, 3, a\rangle &\rightarrow -|0, 3, a\rangle & |0, 3, b\rangle &\rightarrow |0, 3, b\rangle \\
 |3, 0, a\rangle &\rightarrow |3, 0, a\rangle & |3, 0, b\rangle &\rightarrow -|3, 0, b\rangle \\
 |3, 3, a\rangle &\rightarrow |3, 3, a\rangle & |3, 3, b\rangle &\rightarrow |3, 3, b\rangle.
 \end{aligned} \tag{7}$$

In this way we can realise the CZ gate for photons (Eq. (3)) provided we identify the logical qubits:

$$\begin{aligned}
 \text{mode 1:} & & |0\rangle &\rightarrow \text{'1'}, & |3\rangle &\rightarrow \text{'0'} \\
 \text{mode 2:} & & |0\rangle &\rightarrow \text{'0'}, & |3\rangle &\rightarrow \text{'1'}.
 \end{aligned}$$

However, this immediately raises a number of issues relating to the use of a higher Fock state  $|3\rangle$ , such as decoherence, and how to initialise the qubits efficiently and how to perform single qubit rotations? For these reasons we take a different approach.

### III. MULTIPHOTON LOGIC

To bring about solutions, or near solutions to these problems mentioned at the end of the previous section we will make an adaptation to the scheme presented there. This adaptation is to encode our cavity qubits as dual-mode cavity qubits [14]. The more familiar term “dual-rail” seems inappropriate here as the qubits are not flying and there is no rail. The dual mode qubits are formulated, for example, as shown in Table I. In this

| EM Modes             |           | Logical qubit |
|----------------------|-----------|---------------|
| $ 1\rangle 0\rangle$ | $\mapsto$ | $ 1\rangle$   |
| $ 0\rangle 1\rangle$ | $\mapsto$ | $ 0\rangle$   |

TABLE I. Dual-mode qubit coding of the type used in this section.

approach a qubit state is always encoded with a single excitation, as in the dual rail approach [5, 8, 15] and this ensures that if a cavity decay process takes place, we have:  $|1\rangle|0\rangle \rightarrow |0\rangle|0\rangle$ , and then the result is not a valid qubit in this encoding. The difference between the two logical qubit states is where the excitation of the two modes is located, as indicated in Fig. 2.

A consequence of using the dual-mode approach is that in order to have a two-qubit gate we need to have an interaction of an atom with *four* cavity modes, which is

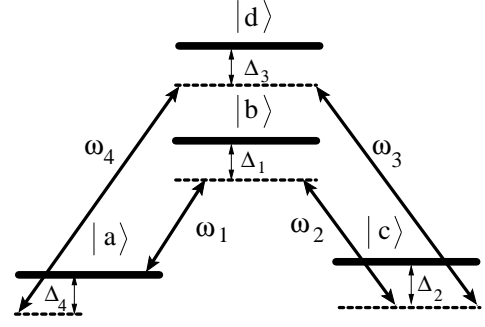


FIG. 3. Scheme of two-qubit iSWAP gate, where  $\omega_i$  (with  $i = 1, 2, 3, 4$ ) are modes of the four-mode high  $Q$  cavity, and  $|a\rangle$ ,  $|b\rangle$ ,  $|c\rangle$ , and  $|d\rangle$  are four energy levels of the atom.

quite demanding (as we shall see), and it is this which we investigate below. As in the simple two-mode system of section II and Hamiltonian (4), we will achieve this by having a sequence of off-resonant interactions with a multilevel atom (Fig. 3), and, as in section II, that atom will be an ancilla which will not be entangled with the final result of a gate operation. The aim of the off-resonant interactions is to reduce spontaneous emission from the ancilla atom. In order that we do not extract “information” from the system via the ancilla atom it is important for the sequence of atomic transitions to start and end on the atomic state  $|a\rangle$  (see Fig. 3). Multiphoton resonance will also require the final detuning,  $\Delta_4$  to ensure resonance. This will mean  $\Delta_4 \approx 0$ , but it has to be optimised for level shifts as we see below.

The full Hamiltonian of the four-level system is then [11, 16]:

$$\begin{aligned}
 H = & \sum_{i=a,b,c,d} \omega_i \hat{\sigma}_{ii} + \sum_{j=1}^4 \omega_j \hat{a}_j^\dagger \hat{a}_j \\
 & + [g_1^{ab} \hat{a}_1 \hat{\sigma}^{ba} + g_2^{bc} \hat{\sigma}^{cb} \hat{a}_2^\dagger + g_3^{cd} \hat{a}_3 \hat{\sigma}^{dc} + g_4^{da} \hat{\sigma}^{ad} \hat{a}_4^\dagger \\
 & + \text{h.c.}],
 \end{aligned} \tag{8}$$

where the first two terms represent the non-coupling Hamiltonians, and the remaining terms describe the atom-field interaction Hamiltonian. The four key initial states of the system and their mappings can be summarised as

$$\begin{aligned}
 & \text{physical} & \text{logical} \\
 |a, 0110\rangle & \mapsto & |a, 00\rangle \\
 |a, 0101\rangle & \mapsto & |a, 01\rangle \\
 |a, 1010\rangle & \mapsto & |a, 10\rangle \\
 |a, 1001\rangle & \mapsto & |a, 11\rangle.
 \end{aligned} \tag{9}$$

In the case of the initial state  $|a, 1010\rangle$ , the system (atom+field) is governed by the Hamiltonian  $H'$  which can be expressed, in the matrix representation and with  $|a, 1010\rangle$  to be the zero-point energy, as

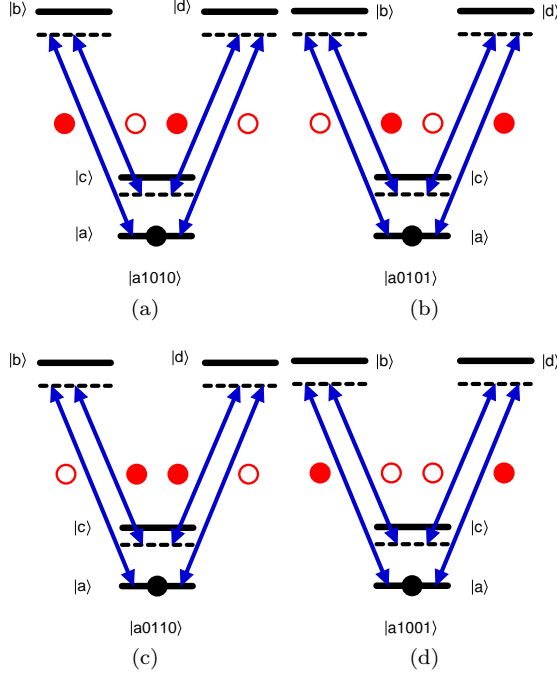


FIG. 4. The four key initial states of the system with possible interactions. Empty red circles represent empty cavity modes and filled red circles represent cavity modes with a single excitation. The filled black circles indicate where the atomic population is located in this simplified analysis of the gate process. Starting from atomic state  $|a\rangle$  we can see that (a) and (b) can progress, but (c) and (d) are blocked.

$$H' = \begin{pmatrix} 0 & g_1^{ab} & 0 & 0 & 0 \\ g_1^{ab} & \Delta_1 & g_2^{bc} & 0 & 0 \\ 0 & g_2^{bc} & \Delta_2 & g_3^{cd} & 0 \\ 0 & 0 & g_3^{cd} & \Delta_3 & g_4^{da} \\ 0 & 0 & 0 & g_4^{da} & \Delta_4 \end{pmatrix}, \quad (10)$$

in the basis states  $\{|a\ 1010\rangle, |b\ 0010\rangle, |c\ 0110\rangle, |d\ 0100\rangle, |a\ 0101\rangle\}$ .

Should we start with different logical qubits, i.e. different arrangements of the excited modes, the multiphoton process is blocked in the case of  $|a\ 0110\rangle$ . In Fig. 4(c) there is no cavity photon available in the first and last modes to raise the atomic state from  $|a\rangle$ . When the initial state is  $|a\ 1001\rangle$ , on the other hand, the evolution of the system is governed by the Hamiltonian  $H''$  given as

$$H'' = \begin{pmatrix} \Delta_2 & g_2^{bc} & 0 & 0 & 0 \\ g_2^{bc} & \Delta_1 & g_1^{ab} & 0 & 0 \\ 0 & g_1^{ab} & 0 & g_4^{da} & 0 \\ 0 & 0 & g_4^{da} & (\Delta_3 - \Delta_4) & g_3^{cd} \\ 0 & 0 & 0 & g_3^{cd} & (\Delta_2 - \Delta_4) \end{pmatrix} \quad (11)$$

acting in the basis states  $\{|c\ 0101\rangle, |b\ 0001\rangle, |a\ 1001\rangle, |d\ 1000\rangle, |c\ 1010\rangle\}$ .

The way the multiphoton process works to shuffle cavity excitation can be seen from Fig. 5. An initial state is

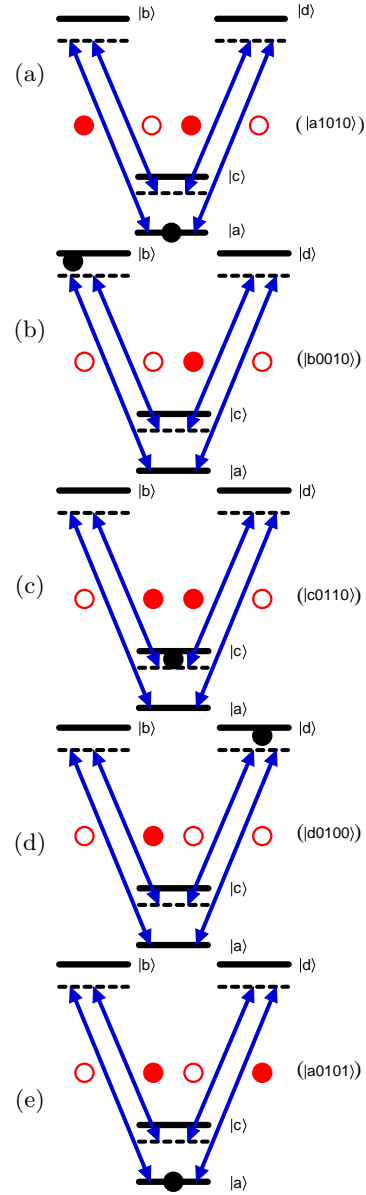


FIG. 5. Sequence of steps for the shuffling excitation amongst four cavity modes. This shuffling realises the swapping part of a gate operation, i.e.  $|a\ 1010\rangle \leftrightarrow |a\ 0101\rangle$ .

set up in Fig. 5(a) where the first and third modes are excited and the second and fourth are not and the atom is in state  $|a\rangle$ . Moving to Fig. 5(b) the atom state moves to  $|b\rangle$  by means of the absorption of a photon from the first mode. Subsequently this can be emitted into the second mode, Fig. 5(c), as the atom approaches the off-resonant state  $|c\rangle$ . Figures 5(d) and 5(e) show how the atomic state returns to  $|a\rangle$  by means of a similar process via the off-resonant level  $|d\rangle$ .

#### IV. VARIANTS OF 4 MODES

In this section we will examine several alternate approaches to carrying out the swapping part of the gate. Because the time evolution of the iswap gate exhibited in the following Sec. IV A is extremely slow, we can achieve a speed-up by allowing some of the intermediate states in Fig. 3 to become resonant. However there are a wide range of possibilities which are shown in Fig. 6. Our choice of system needs to be informed by which configurations can keep the qubit state  $|a11\rangle$  in its initial state at the appropriate interaction time.

To easily identify the different model systems we will use a binary type notation to indicate which levels in the sequence of states are to be resonant, and which are not. Thus the Model(10001) in Fig. 6 has only two resonant states in the chain, the first and last ones, and will be treated in Eq. (13). If we took a fully resonant model, where every transition is resonant, the model would be Model(11111) also shown in Fig. 6. In the next section we will focus on Model(11001), as one of the cases with three resonant levels, i.e. it has two intermediate resonant levels.

##### A. An effective two-level system

For the initial state  $|a\ 1010\rangle$ , the effective wavefunction of the system can be expressed as:

$$|\Psi(t)\rangle = c_1|a1010\rangle + c_2|b0010\rangle + c_3|c0110\rangle + c_4|d0100\rangle + c_5|a0101\rangle. \quad (12)$$

which is a superposition of the key states used for single photon swapping.

In Appendix A we will utilize a theory for the adiabatic elimination of the unwanted (off-resonant) levels as shown in Fig. 3. Thus using the basis of Eq. (12) we will develop an effective two-level Hamiltonian which takes the form

$$H_{\text{eff}} = \begin{bmatrix} 0 & g_{\text{eff}} \\ g_{\text{eff}} & \Delta_{\text{eff}} \end{bmatrix}, \quad (13)$$

where  $(g \ll \Delta)$  is required (see appendix B1). The effective coupling is found to be

$$g_{\text{eff}} \approx -\frac{g_1^{\text{ab}} g_2^{\text{bc}} g_3^{\text{cd}} g_4^{\text{da}}}{\Delta_1 \Delta_2 \Delta_3}, \quad (14)$$

and the effective detuning of the two-level system is

$$\Delta_{\text{eff}} \approx \Delta_4 + \frac{(g_1^{\text{ab}})^2}{\Delta_1} - \frac{(g_4^{\text{da}})^2}{\Delta_3}. \quad (15)$$

The time evolution of this system is given by the following equations for the logical states,

$$\begin{aligned} |a, 10\rangle &\mapsto \cos(g_{\text{eff}} t) |a, 10\rangle - i \sin(g_{\text{eff}} t) |a, 01\rangle \\ |a, 01\rangle &\mapsto \cos(g_{\text{eff}} t) |a, 01\rangle - i \sin(g_{\text{eff}} t) |a, 10\rangle. \end{aligned} \quad (16)$$

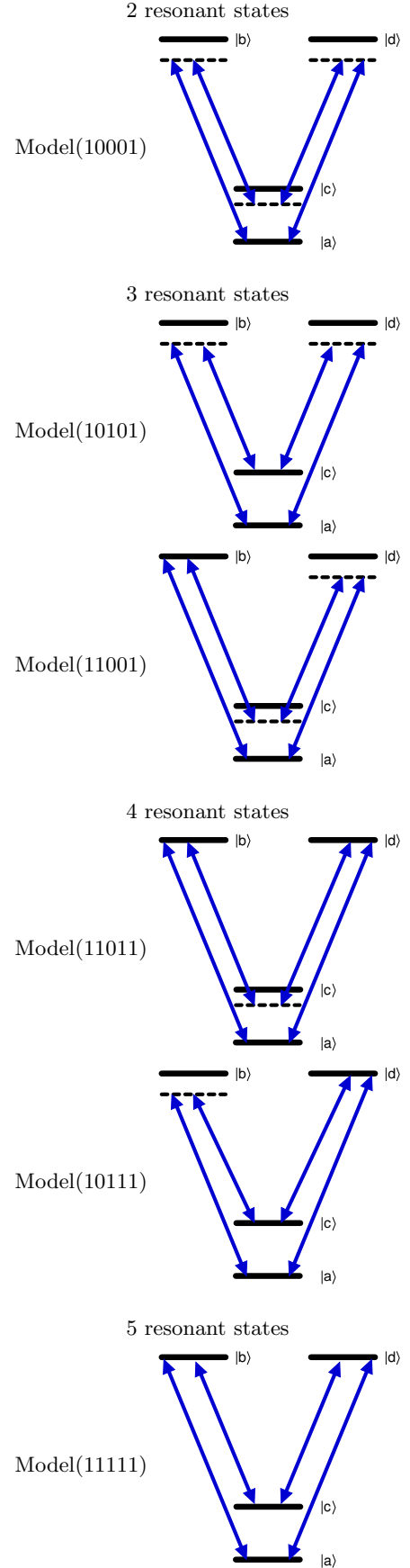


FIG. 6. Linkage schemes for 4 modes  $N$  resonant states (with  $N=1, 2, 3, 4, 5$ ).

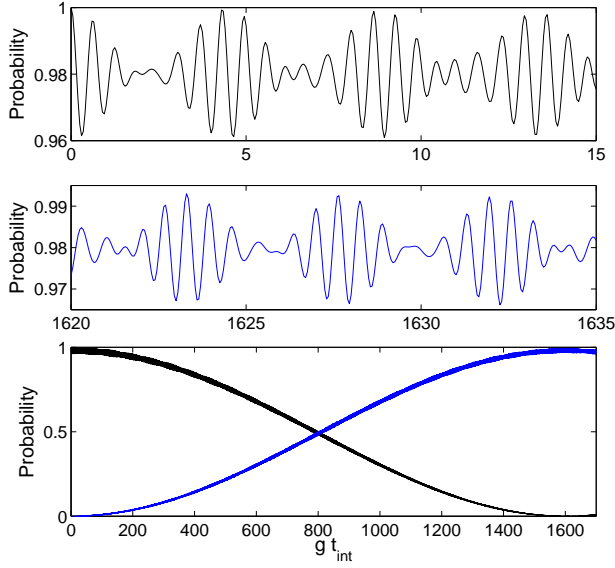


FIG. 7. Population swapping in the model (10001). All couplings  $g_j$  ( $j = 1, 2, 3, 4$ ) are set to  $g$ , and the detunings  $\Delta_i$  with  $i = 1, 2, 3$  are set to  $\Delta$ . The value of  $\Delta_4$  is determined by Eq. (15).

This two-level system undergoes swapping of the states  $|a1010\rangle$  and  $|a0101\rangle$  when the resonance condition is achieved by setting  $\Delta_{\text{eff}}$  to zero in equation (15). This is illustrated in Fig. 7 where excellent agreement between an exact numerical calculation and the analytic treatment of equations (16) is presented. Because of the finite value of  $\Delta$  chosen in Fig. 7 a fine high frequency oscillation can be seen. For larger detuning this oscillation becomes smaller as the two-level approximation is realised more accurately.

The effective Hamiltonian (13) only connects the states  $|a1010\rangle$  and  $|a0101\rangle$ ; the state  $|a1001\rangle$  is effectively governed instead by the full Hamiltonian (11), and the other logical state of the system,  $|00\rangle$ , is unchanged. Considering the parameters in Fig. 7 and at the special time  $|g_{\text{eff}}t| = \pi/2$ , we obtain the following outputs for the basic inputs (see Fig. 8):

| Input        | Output        |
|--------------|---------------|
| $ 00\rangle$ | $ 00\rangle$  |
| $ 01\rangle$ | $i 10\rangle$ |
| $ 10\rangle$ | $i 01\rangle$ |
| $ 11\rangle$ | $ 11\rangle$  |

(17)

This realises an iSWAP gate and we can represent the above mappings as the table

$$\text{iSWAP} \equiv \begin{bmatrix} 1 & & & \\ & 0 & i & \\ & i & 0 & \\ & & & 1 \end{bmatrix}. \quad (18)$$

The iSWAP gate is a universal gate when combined with single qubit rotations. For example it can be directly related to the CNOT gate (also a universal gate) by means of

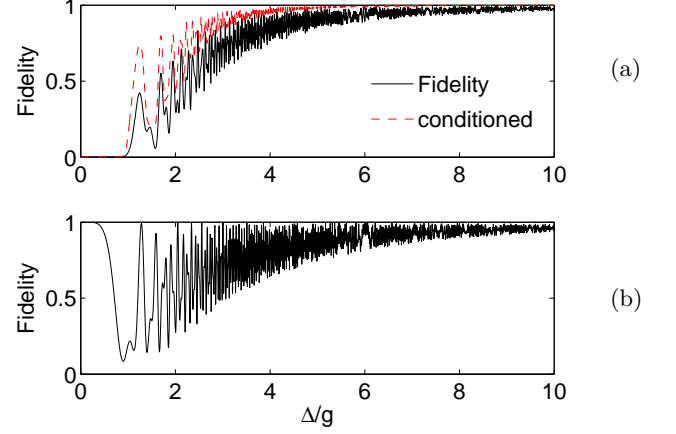


FIG. 8. (a) The fidelity (black line) of swapping the logical states  $|a10\rangle$  and  $|a01\rangle$  in the model (10001). Red-dashed line shows the conditional fidelity. (b) The fidelity of keeping the system initially in the logical state  $|a11\rangle$ . Parameters of the detunings  $\Delta$  and the coupling strengths  $g$  are defined in Fig. 7.

a quantum circuit as shown in [17]. Recently, it is shown that the iSWAP gate can be very useful for applications in quantum information process QIP and quantum computing. For example, it is reported that the replacement of the standard CNOT gate by the iSWAP gate provides more efficient, simpler, and faster way of generating cluster states [18], which play a crucial role in the so-called one-way quantum computation approach [19, 20].

### B. A three-level behaviour

Model (11001) has an intermediate resonant state. The system takes the form of a double  $\Lambda$  system with a common initial and final state. Since  $|b0010\rangle$  is taken to be resonant, we apply the adiabatic elimination theory (as shown in appendix B2) to obtain an effective three-level system in the reduced space of states  $\{|a1010\rangle, |b0010\rangle, |a0101\rangle\}$ . The effective couplings are found to be

$$g_{\text{eff}}^{(1)} = g_1^{\text{ab}}, \quad g_{\text{eff}}^{(2)} \approx \frac{g_2^{\text{bc}} g_3^{\text{cd}} g_4^{\text{da}}}{\Delta_2 \Delta_3}, \quad (19)$$

and the effective detunings

$$\begin{aligned} \Delta_{\text{eff}}^{(1)} &\approx \Delta_1 - \frac{(g_2^{\text{bc}})^2}{\Delta_2}, \\ \Delta_{\text{eff}}^{(2)} &\approx \Delta_4 - \frac{(g_4^{\text{da}})^2}{\Delta_3}. \end{aligned} \quad (20)$$

The resulting Hamiltonian takes the form

$$H_{\text{eff}} = \begin{bmatrix} 0 & g_{\text{eff}}^{(1)} & 0 \\ g_{\text{eff}}^{(1)} & \Delta_{\text{eff}}^{(1)} & g_{\text{eff}}^{(2)} \\ 0 & g_{\text{eff}}^{(2)} & \Delta_{\text{eff}}^{(2)} \end{bmatrix}. \quad (21)$$



The time evolution of this gate is shown in Fig. 9(a) and it is immediately apparent that the population swapping happens much faster than the evolution seen in Fig. 7 for Model (10001). The time evolution of the swapping follows the equations (for the initial state  $|a, 1010\rangle$ )

$$\begin{aligned} |a, 10\rangle \longrightarrow & \left[ \frac{(g_{\text{eff}}^{(1)})^2}{\bar{g}^2} + \frac{(g_{\text{eff}}^{(2)})^2}{\bar{g}^2} \cos(\bar{g}t) \right] |a, 10\rangle \\ & - i \frac{g_{\text{eff}}^{(1)}}{\bar{g}} \sin(\bar{g}t) |\Phi\rangle \\ & + \frac{g_{\text{eff}}^{(1)} g_{\text{eff}}^{(2)}}{\bar{g}^2} [\cos(\bar{g}t) - 1] e^{i\eta t} |a, 01\rangle, \end{aligned} \quad (22)$$

where  $\bar{g} = \sqrt{(g_{\text{eff}}^{(1)})^2 + (g_{\text{eff}}^{(2)})^2}$  and  $|\Phi\rangle \equiv |b, 0010\rangle$ .

The spin- $J$  model predicts the proper values for the effective coupling constants so that a complete qubit swapping can be achieved. That is, in the previous three-level system, the general scaling expression [21]

$$g_{\text{eff}}^{(n)} = g_0 \sqrt{n(N-n)} \quad (23)$$

(where  $g_0$  is a constant and in our case  $N = 3$  and  $n = 1, 2$ ) suggests that  $|g_{\text{eff}}^{(1)} t| = |g_{\text{eff}}^{(2)} t| = \pi/\sqrt{2}$ . Then, the transformation  $|a, 1010\rangle \rightarrow \exp(i\eta t)|a, 0101\rangle$  can take place by setting  $\bar{g}t = \pi$ . A global phase  $\eta t$  in the previous two- and three-level systems can be produced by following different proposals. Some examples will be suggested when we discuss the single-qubit gate in Sec. VD.

By substituting the parameters of the coupling constants and detunings in the model (11001) into the Hamiltonian (11) which describes the time evolution of the initial state  $|a, 1001\rangle$ , it is noticeable that this state can be sufficiently forced to stay in its initial state, as demonstrated by the red-dashed line in Fig. 9(b).

### C. Enhancement conditional on measurements

In the scheme we have developed so far the atom plays the role of an ancilla which simply “enables” the shuffling of energy between cavity modes. However, if the proposed gate is slightly imperfect there will be a small admixture of other atomic states. The role of a conditional measurement can be to improve the quality of the final state (i.e. to improve the fidelity). For example, let us suppose the state of the system is

$$|\Psi(t)\rangle = c_1|a, 1010\rangle + c'|c, 0110\rangle + c_2|a, 0101\rangle + \dots \quad (24)$$

Then if the atom exits the system in state  $|a\rangle$  we must project the state (24) onto the atomic state  $|a\rangle$  to obtain the conditioned result

$$|\Psi(t)\rangle' \rightarrow \frac{c_1}{\sqrt{|c_1|^2 + |c_2|^2}} |a, 1010\rangle + \frac{c_2}{\sqrt{|c_1|^2 + |c_2|^2}} |a, 0101\rangle. \quad (25)$$

Because of the renormalisation that takes place this conditionally enhances a desired result (such as  $|a, 0101\rangle$ ).

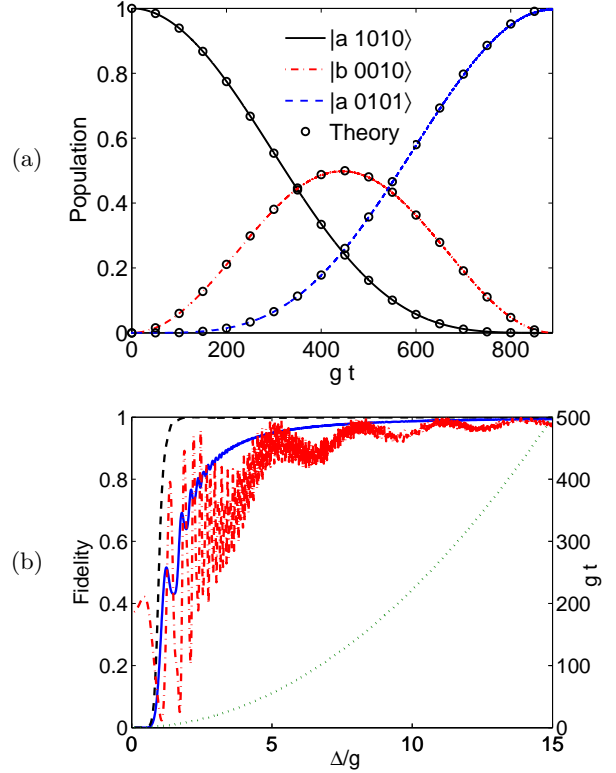


FIG. 9. [Color online] A three-level behaviour with the states  $|c\rangle$  and  $|d\rangle$  chosen to be highly-detuned (see Fig. 3). Parameters: the coupling constants  $g_{2,3,4}$  are all set to  $g$ , and the detunings  $\Delta_{2,3}$  are set to  $\Delta$ . (a) the probability of the states  $|a, 1010\rangle$ ,  $|b, 0010\rangle$ , and  $|a, 0101\rangle$  with  $\Delta = 20g$ . (b) the fidelity of mapping  $|a, 10\rangle$  to  $|a, 01\rangle$  (blue-solid line), and of keeping  $|a, 11\rangle$  in its initial state (red dotted-dashed line). The black-dashed and green-dotted lines represent the conditioned fidelity and the interaction time  $gt_{\text{int}}$ , respectively.

To a limited extent this makes the scheme probabilistic. However, the probability of success in such a measurement is expected to be high and the intent is that this measurement process simply enhances the result and cleans up the wave-function. Red-dashed line in Fig. 8(a) and black-dashed line in Fig. 9(b) show significant improvement of fidelity in the models (10001) and (11001).

### D. Decoherence process

The time evolution of the previous systems can be governed by Liouville's equation

$$\frac{\partial}{\partial t} \rho = -i[H, \rho] + \mathcal{L} \rho, \quad (26)$$

where  $\rho$  is the density operator of the atom-field system and the so-called Liouvillian operator  $\mathcal{L}\rho$  describes the dissipative mechanisms in the system. The general Lindblad form of the Liouvillian operator  $\mathcal{L}\rho$  can be expressed

as [22]

$$\mathcal{L} \rho = \sum_i \frac{\eta_{(i)}}{2} ([L_{(i)} \rho, L_{(i)}^\dagger] + [L_{(i)}, \rho L_{(i)}^\dagger]), \quad (27)$$

where  $\eta$  represents the loss of population which can be due to either the spontaneous emission  $\Gamma$  or to the cavity field rate  $\kappa$ . The operators  $L$  and  $L^\dagger$  are the corresponding system operators. More explicitly, in the presence of the atomic decay  $L$  and  $L^\dagger$  can be replaced by the atomic operators  $\sigma_-$  and  $\sigma_+$ , and in the case of the cavity decay they are represented by the field operators  $a$  and  $a^\dagger$ .

Given the initial states to be either  $|a\ 1010\rangle$  or  $|a\ 0101\rangle$ , we can also investigate the influence of the atomic and photonic relaxations by considering the following Hamiltonian

$$H' = H - i \frac{\kappa}{2} \sum_{i=1}^4 a_i^\dagger a_i - i \frac{\Gamma}{2} (|b\rangle\langle b| + |d\rangle\langle d|), \quad (28)$$

where  $H$  is the original Hamiltonian of the system in the absence of any decay.

This procedure is valid under the condition that no photon is detected [23–25], and the Shore's method [26] can be reapplied to produce the damped N-level configurations. We have seen previously that the models (10001) and (11001) are capable to realise the iSWAP gate. Starting with the model (10001), the time evolution of the

state  $|a\ 0101\rangle$  in the strong coupling regime is

$$c_{a01}(t) = -i \frac{g_{\text{eff}}}{\tilde{g}} e^{-\kappa t} \sin(\tilde{g}t) e^{-i\Delta_{\text{eff}}t/2}, \quad (29)$$

where  $\tilde{g} = \sqrt{g_{\text{eff}}^2 + (\Delta_{\text{eff}}/2)^2}$ . The norm of the system shows that it decays with the rate  $(2\kappa)$ . Figure 10(a) demonstrates the fidelity for different values of  $\kappa$ . As we have mentioned before, the iSWAP gate formed from the model (10001) is very slow gate and, therefore, it is very sensitive to photonic decay rates.

In the case of the model (11001) and taking into account the atomic and cavity decay rates in the effective Hamiltonian (21), the eigenvalues for this effective Hamiltonian can be determined, under the condition  $4\bar{g} \geq (\kappa - 2\Gamma)$  and with vanishing effective detunings, as

$$\lambda_1 = -\kappa, \quad \lambda_{2,3} = -\left(\frac{3\kappa + 2\Gamma}{4}\right) \pm i\lambda, \quad (30)$$

where  $\lambda = \{\bar{g}^2 - \frac{1}{4}(\kappa - 2\Gamma)^2\}^{1/2}$ ,  $\bar{g} = \sqrt{(g_{\text{eff}}^{(1)})^2 + (g_{\text{eff}}^{(2)})^2}$ , and  $g_{\text{eff}}^{(1)}$  and  $g_{\text{eff}}^{(2)}$  are the effective coupling constants. The corresponding eigenvectors can be found and then the time evolution of the logical state  $|a\ 01\rangle$  can be expressed as

$$c_{a01}(t) = \frac{g_{\text{eff}}^{(1)} g_{\text{eff}}^{(2)}}{\bar{g}^2} \exp(-\kappa t) \left\{ -1 + \left[ \cos(\lambda t) - \left(\frac{\kappa - 2\Gamma}{4\lambda}\right) \sin(\lambda t) \right] \exp\left(\frac{\kappa - 2\Gamma}{4} t\right) \right\}, \quad (31)$$

for the initial condition that the system is completely set in the initial state  $|a\ 1010\rangle$  at  $t = 0$ , i.e.  $c_{a10}(0) = 1$ .

In Fig. 10(b) we consider the model (11001) and measure the fidelity at different values of  $\kappa$ . Figure 10 shows that the impact of cavity field relaxation is less in the model (11001) when compared to the model (10001), and this is because of the improvement in the qubit states speed.

In the case of the initial state to be  $|a\ 0110\rangle$ , this state decays due to the cavity relaxation and the population loss follows  $|c_{a00}|^2 = \exp(-2\kappa t_{\text{int}})$ , where the interaction time  $t_{\text{int}}$  is same to the models (10001) and (11001). In the final state  $|a\ 001\rangle$  we directly use the master equation (26) to investigate the effect of atomic and photonic dampings in either the model (10001) or the model (11001).

We are now in the position to subject all qubit states in the iSWAP gate to experimental values including the coupling strength  $g$ , the atomic decay  $\Gamma$ , and the photonic decay rate  $\kappa$  so that the performance of the two-qubit dual-rail CQED gate can be practically tested. Considering the microwave cavity-QED experiment in [27], highly excited Rydberg atoms (typically  $^{85}\text{Rb}$ ) with a radiative time  $\tau_{\text{rad}} \sim 30$  ms have been used to interact with a

superconducting cavity with  $Q \mapsto 4 \times 10^{10}$ . The photon lifetime inside the cavity is in order  $\tau_{\text{ph}} \sim 130$  ms, and the coupling strength is around  $g/2\pi \sim 50$  kHz. By setting  $\Delta = 10$  g, this corresponds to cavity-atom interaction time  $t_{\text{int}} \mapsto 5$  ms in the configuration (10001), and  $t_{\text{int}} \mapsto \frac{1}{\sqrt{2}}$  ms in the configurations (11001). The quantity  $\tau_{\text{ph}}/t_{\text{int}}$  shows that the last configuration is much better for QIP applications with the present cavity QED techniques. Plots in Fig. 11 show the population loss in the iSWAP gate realised by the configurations (10001) and (11001) with considering the above values of the parameters  $g$ ,  $\Gamma$ , and  $\kappa$ .

### V. THREE QUBIT GATES AND ROTATIONS

So far we have described a two-qubit entangling gate. However, to have a universal set of gate operations it is necessary to have single qubit rotations (or single qubit gates). We also present below a three qubit gate, where full details will be presented in appendices C and D.



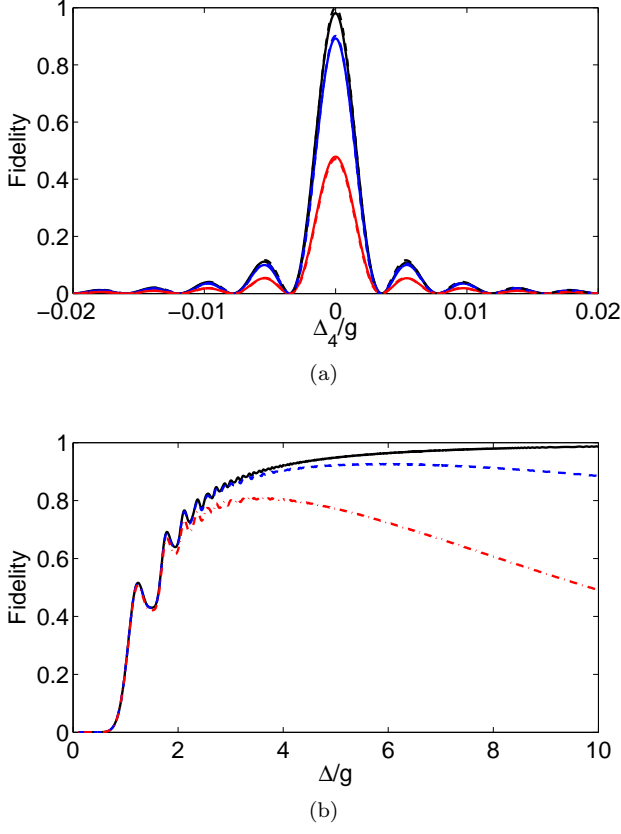


FIG. 10. The influence of the dissipative mechanisms on the qubit state  $|a\ 10\rangle$  or  $|a\ 01\rangle$  in the models (10001) and (11001). (a) in the model (10001), the three curves corresponding to the values of photonic decays  $\kappa \sim (0, 0.033, 0.24)g_{\text{eff}}$  with  $\Delta = 10g$ . The solutions by theory (dashed lines) and simulation (solid lines) are highly matched. (b) in the model (11001) The three curves corresponding to the values of the atomic decay rates  $\Gamma \sim (0, 0.1, 0.75)\bar{g}/\sqrt{2}$  with  $\kappa = 0$ , or to the values of photonic decays  $\kappa \sim (0, 0.025, 0.185)\bar{g}/\sqrt{2}$  when no atomic decay rate is considered. The three curves in all these plots represent (100, 90, 50)% fidelity.

### A. Three qubit gate

The three qubit scheme of Fig. 15 contains dual-mode qubits with a repeated mode at  $\omega_1$ . The partner mode for  $\omega_1$  is not shown as it is unaffected by the logic process. The remaining pairs are  $\omega_{2,3}$  and  $\omega_{5,6}$ , (a mode with the label  $\omega_4$  is omitted in the following analysis to avoid confusion). The consequence of the repeated mode 1 is that the chain only completes if mode 1 is present (in which case the excitation is absorbed and then re-emitted) and if modes 3 and 5 have excitations present (which implies necessary empty modes 2 and 6 in the dual-mode qubit basis). The result of all this is that the qubit 1 acts as a control qubit which swaps the qubits present in logical qubits 2 and 3: i.e. we have the logic needed for a Fredkin gate [28]. In a Fredkin gate we aim for logical qubits to be mapped as follows:

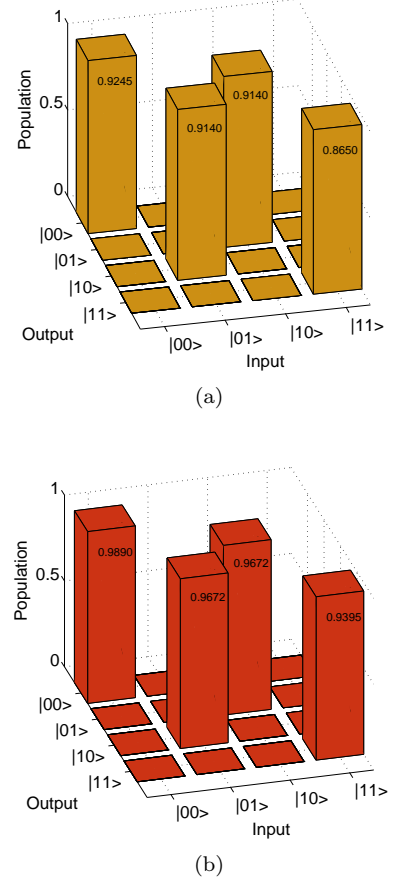


FIG. 11. Truth table of the numerically simulated iSWAP gate with  $\Delta = 10g$  in the presence of decoherence processes. (a) in the configuration (10001). (b) in the model (11001). Parameters: the coupling constant is approximate  $g/2\pi = 50$  kHz,  $\Gamma/g \sim 10^{-4}$ , and  $\kappa/g \sim 2.5 \times 10^{-5}$ .

| Input         | Output        |
|---------------|---------------|
| $ 000\rangle$ | $ 000\rangle$ |
| $ 001\rangle$ | $ 001\rangle$ |
| $ 010\rangle$ | $ 010\rangle$ |
| $ 011\rangle$ | $ 011\rangle$ |
| $ 100\rangle$ | $ 100\rangle$ |
| $ 110\rangle$ | $ 101\rangle$ |
| $ 101\rangle$ | $ 110\rangle$ |
| $ 111\rangle$ | $ 111\rangle$ |

(32)

The Fredkin gate is a universal gate owning important properties which set up the general principles of logic gates and circuits in both classical and quantum computing [28]. This gate swaps the second and the third qubits if the first qubit is  $|1\rangle$ , otherwise, all qubits remain unchanged. Two examples of quantum circuits generating this gate can be considered. Firstly, it is observable that the Fredkin gate is nothing but the controlled SWAP gate [29]. Secondly, since the SWAP gate is equivalent to three CNOT gates, we can see that the Fredkin gate is a

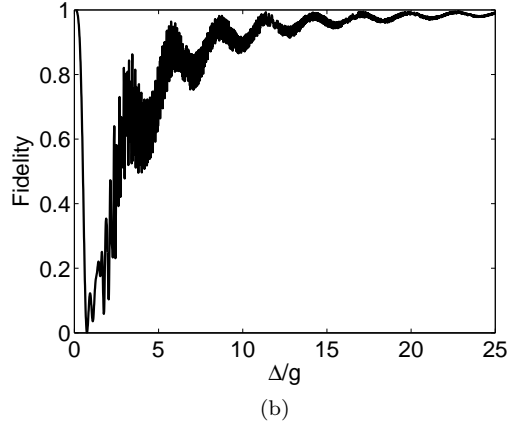
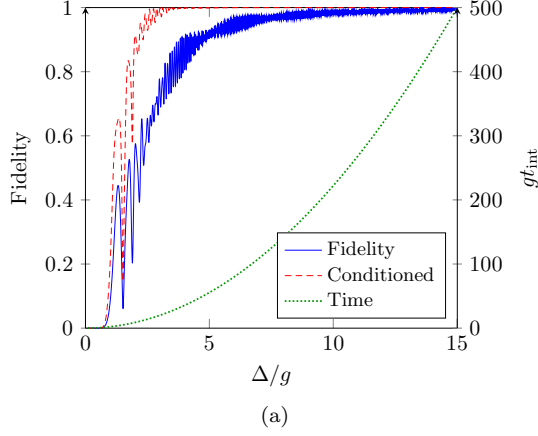


FIG. 12. Fidelity for the fast Fredkin gate shown as a function of the detuning  $\Delta$  where we again take  $\Delta_j \rightarrow \Delta$  for  $j = 1, 2, 4, 5$  with  $\Delta_3 = 0$  and  $\Delta_6 \sim 0$  (given by equation (34) set to zero). The initial state is (a)  $|a 101\rangle$ , (b)  $|a 100\rangle$ . For the couplings we take  $g_j \rightarrow g$ . The dashed line in (a) shows the interaction time  $\bar{g}t_{\text{int}} = \pi$  as found from the three-state model IV B.

combination of the Toffoli gate together with two CNOT gates [30].

### B. Two- and three-level configurations

For a de-excited atom interacting with multimode cavities, the realisation of the Fredkin gate at the interaction time  $gt_{\text{int}}$  can be achieved when the transformation  $|a 101\rangle \leftrightarrow |a 110\rangle$  is made and the remaining logical qubits are in their initial states. Once again, Shore's method plus the spin- $J$  model provide useful tools to find out several configurations that are capable of swapping the states  $|a 101\rangle$  and  $|a 110\rangle$ . However, to meet the truth table of the Fredkin gate, and since there is a presence of a repeated mode 1 in addition to certain overshoot states (see appendix C) it is noticed that the only possible configurations realising the gate are the models (1000001) and (1001001). In the model (1000001) we set

all states other than the states  $|a 101\rangle$  and  $|a 110\rangle$  to be far-resonance, and in the model (1001001) a further atomic state  $|d\rangle$  is allowed to be resonant. The full details of the analysis of the former model (1000001) are not presented here, it can be found in [14] where we also show that an excellent speed-up is obtained by chosen an intermediate resonant energy level, i.e. the model (1001001). In this case the effective Hamiltonian reduces to a three-level system again, where (see appendix C) the effective coupling constants are

$$g_{\text{eff}}^{(1)} = \frac{g_1^{\text{ab}} g_2^{\text{bc}} g_3^{\text{cd}}}{\Delta_1 \Delta_2}, \quad g_{\text{eff}}^{(2)} = \frac{g_1^{\text{de}} g_5^{\text{ef}} g_6^{\text{fa}}}{\Delta_4 \Delta_5}, \quad (33)$$

and the effective detunings are

$$\Delta_1^{\text{eff}} \approx \Delta_3 + \frac{(g_1^{\text{ab}})^2}{\Delta_1} - \frac{(g_3^{\text{cd}})^2}{\Delta_2} - \frac{(g_1^{\text{de}})^2}{\Delta_4}, \quad (34)$$

$$\Delta_2^{\text{eff}} \approx \Delta_6 - \frac{(g_6^{\text{af}})^2}{\Delta_5}.$$

Given the initial state to be either the logic  $|a 101\rangle$  or  $|a 110\rangle$ , equations of motion in (22) and the sequence of effective Rabi frequencies in (23) can be reused to swap the qubit states  $|a 10\rangle$  and  $|a 01\rangle$ . A high fidelity result can be obtained for sufficient detunings, Fig. 12(a) shows how this increases, and also how the use of measurement of the ancilla atom strongly improves the result for the quite low value of  $\Delta/g \gtrsim 3$ . The same Fig. shows the interaction time which is fairly high for large  $\Delta$  ( $gt \sim 500$  for  $\Delta = 15g$ ) but reduces substantially near  $\Delta = 5g$ . The fidelity for keeping the qubit state  $|a 100\rangle$  in its initial state at the same interaction time above has been illustrated in Fig. 12(b). For other qubit states, large detunings for all atomic levels except  $|a\rangle$  and  $|d\rangle$  ensure an efficient confinement of the populations in desired levels so that the three-qubit Fredkin gate is built.

### C. Decoherence in fast Fredkin gate

Considering the parameters of the coupling constants and the detunings in the model (1001001) given by Eqs. (33, 34), we can use the master equation (26) to address the influence of atomic and photonic relaxations on the Fredkin gate. Furthermore, we can use the conditional Hamiltonian (28) to find analytic solutions for certain qubit states in Fredkin gate. For example, the damping due to atomic and photonic decays can be studied as follows. Under the strong coupling regime, the eigenvalues of the damped three-level behaviour (1001001) can be given as

$$\lambda_1 = -3\kappa/2, \quad \lambda_{2,3} = -\left(\frac{5\kappa + 2\Gamma}{4}\right) \pm i\lambda, \quad (35)$$

where  $\lambda = \left(\bar{g}^2 - \frac{1}{4}(\kappa - 2\Gamma)^2\right)^{1/2}$ ,  $\bar{g} = \sqrt{(g_{\text{eff}}^{(1)})^2 + (g_{\text{eff}}^{(2)})^2}$ , and  $g_{\text{eff}}^{(1)}$  and  $g_{\text{eff}}^{(2)}$  are given by Eq. (33) and the effective

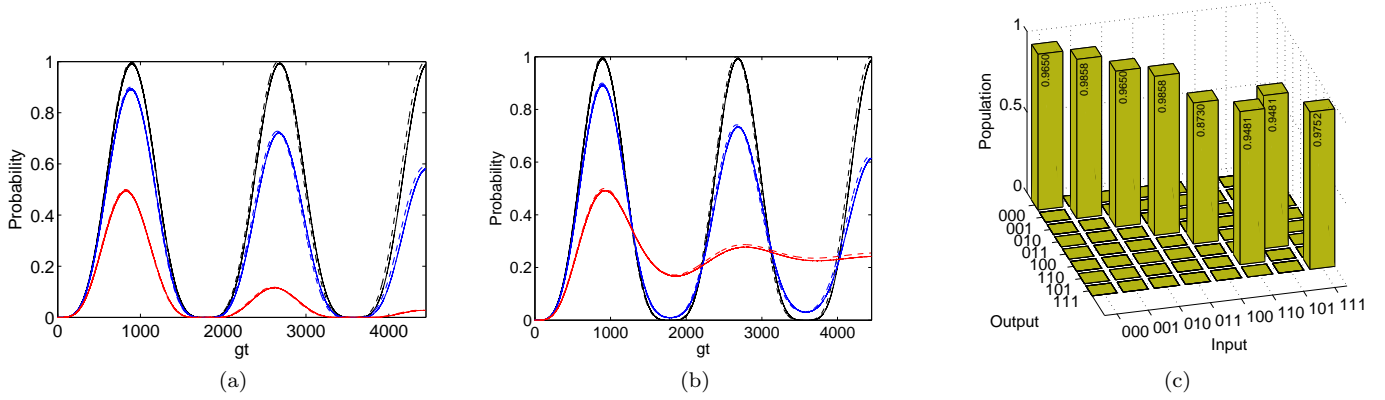


FIG. 13. In (a) and (b) the probability of the qubit state  $|a 110\rangle$  in the model (1001001) with non-vanishing photonic and atomic decays. Solid and dashed curves show the numerical and theoretical solutions, respectively. The coupling constants  $g_i$  ( $i = 1, 2, 3, 5, 6$ ) all are set to  $g$ , and the detunings  $\Delta_{1,2,4,5} = \Delta$  with  $\Delta = 20g$ . The effective couplings of the truncated system  $g_{\text{eff}}^{(1)}$  and  $g_{\text{eff}}^{(2)}$  are given by Eq. (33), and the detunings  $\Delta_3$  and  $\Delta_6$  are defined by the resonance conditions in Eq. (34). The black, blue, and red lines respectively represent (at the interaction time  $gt_{\text{int}}$ ) the system probability  $P \sim (100, 90, 50)\%P_0$  with a maximum probability  $P_0 \sim 0.9950$ . The three curves corresponding to the values of: (a) the photonic decay rates  $\kappa \sim (0, 0.0174, 0.1186)\bar{g}/\sqrt{2}$  with  $\Gamma \mapsto 0$ , and (b) the atomic decay rates  $\Gamma \sim (0, 0.0976, 0.764)\bar{g}/\sqrt{2}$  with  $\kappa \mapsto 0$ . (c) a truth table of the numerically simulated Fredkin gate with  $\Delta = 10g$  in the presence of decoherence processes. Parameters: the coupling constant is approximately  $g/2\pi = 50$  kHz,  $\Gamma/g \sim 10^{-4}$ , and  $\kappa/g \sim 2.5 \times 10^{-5}$ .

detunings all are set to zero. The time evolution of the

coefficient  $c_{a110}$ , with the initial conditions  $c_{a101}(t=0) = 1$ ,  $c_d(0) = 0$ , and  $c_{a110}(0) = 0$ , reads

$$c_{a110} = \frac{g_{\text{eff}}^{(1)} g_{\text{eff}}^{(2)}}{\bar{g}^2} \exp\left(-\frac{3\kappa}{2} t\right) \left\{ -1 + \left[ \cos(\lambda t) - \left( \frac{\kappa - 2\Gamma}{4\lambda} \right) \sin(\lambda t) \right] \exp\left(\frac{\kappa - 2\Gamma}{4} t\right) \right\}. \quad (36)$$

Figure 13 demonstrates the population loss by either the spontaneous emission  $\Gamma$  or the cavity field decay  $\kappa$ , and the damped Fredkin gate under the recent QIP techniques.

In the absence of  $\Gamma$  it is shown by Eqs. (31, 36) that the Fredkin gate is more sensitive to cavity field decay rate, and the iSWAP and the Fredkin gates in the previous three-level configurations have the same sensitivity to the spontaneous emissions when no photonic decay is considered.

#### D. Single qubit gates

We turn briefly to single qubit rotations which are required to make a universal set of gates. Within the dual-mode scheme a  $\Lambda$ -atom-mode system, such as seen in Fig. 1 cannot be used because for an arbitrary rotation of the mode excitation between the cavity modes the atomic state changes as well. For that reason we add a classical field to allow a return to the original atomic state  $|a\rangle$  (see Fig. 14). Otherwise the scheme is similar to Fig. 1 in that we have a lambda atom which has two transitions coupled to two cavity modes that make up a qubit. We will adiabatically eliminate levels  $|b\rangle$  and  $|c\rangle$  from the inter-

action under the conditions  $\Delta_1, \Delta_2 \gg g_1^{\text{ab}}, g_2^{\text{bc}}, \Omega/2, \Delta_3$  (see appendix D) to find the effective detuning

$$\Delta_{\text{eff}} = \Delta_3 + \frac{(g_1^{\text{ab}})^2}{\Delta_1}, \quad (37)$$

and the effective coupling

$$g_{\text{eff}} = \frac{g_1^{\text{ab}} g_2^{\text{bc}} \Omega}{2\Delta_1 \Delta_2}. \quad (38)$$

We can then ensure a qubit rotation in the form

$$\hat{R}_x(g_{\text{eff}} t) = \cos(g_{\text{eff}} t/2) \hat{I} - i \sin(g_{\text{eff}} t/2) \hat{\sigma}_x. \quad (39)$$

The Pauli Z gate can be easily realized by our qubits, too. Generally speaking, the atom-cavity interaction in the Jaynes-Cummings model shows that for an atom in the ground state  $|g\rangle$  interacting with a single mode having  $n$  photons:

$$|g, n\rangle \mapsto \cos(g\sqrt{n}t)|g, n\rangle - i \sin(g\sqrt{n}t)|e, n-1\rangle.$$

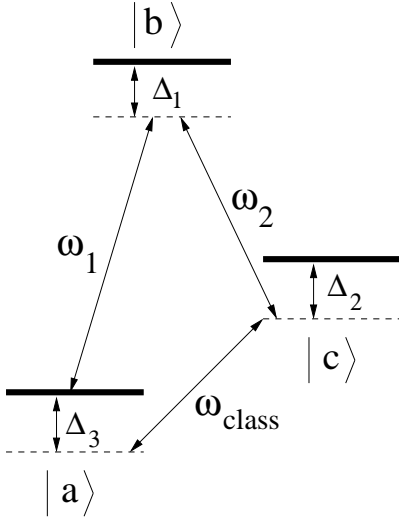


FIG. 14. The model for a single-qubit Pauli-X gate. A three-level atom with  $\Lambda$  configuration of levels interacting with the optical cavity modes  $\omega_1$  and  $\omega_2$  on the transitions  $|a\rangle \leftrightarrow |b\rangle$  and  $|b\rangle \leftrightarrow |c\rangle$ . The transition  $|c\rangle \leftrightarrow |a\rangle$  is coupled by the classical field  $\omega_{\text{class}}$ .

This is the case when the frequencies of the atomic transitions and the mode are equally matched (i.e. the resonance case  $\omega_{eg} = \omega$ ). In the case of very large detuning ( $\Delta \gg g$ ), on the other hand, the system remains in its initial state and a phase shift can be produced as

$$|g, n\rangle \mapsto e^{i\Phi(n)} |g, n\rangle, \quad (40)$$

with  $\Phi(n)$  can be expressed as [31]

$$\Phi(n) = \frac{\Delta}{2v} \int_0^L dz \left[ \sqrt{1 + n \left( \frac{g(z)}{\Delta/2} \right)^2} - 1 \right], \quad (41)$$

where  $v$  is the velocity of the atom passing through a cavity,  $L$  is the cavity length, and  $g(z)$  is the coupling constant which in our case is independent of  $z$ . By setting  $n = 0$  nothing happens, but with a cavity being initially in the number state  $|1\rangle$  (i.e. there is  $n = 1$  photon) a set of phase gates can be realised and the rotation operator  $R_z$  can be produced. In the case of two modes inside the cavity interacting with an atom in the ground state  $|a\rangle$ , such a case in the dual-rail qubits  $|a 10\rangle$  and  $|a 01\rangle$ , the previous argument can be followed to introduce a phase shift. That is, we can set a large detuning between the atom and, say the first mode, and set a very high detuning between the atom and the second mode. In this case, if the excitation is in the first mode, one finds  $|a 10\rangle \mapsto e^{ig^2t/\Delta} |a 10\rangle$ ; otherwise,  $|a 01\rangle \mapsto |a 01\rangle$ .

Different ways can be considered to add a global phase  $\eta t$  to the two- or three-qubit gates already discussed in the previous sections. For instance, the single-qubit phase gate above can be employed for this purpose. That is, in the case of the previous ISWAP gate and after producing the transformations in Sec. IV, an atom initially in the ground state  $|a\rangle$  sent to the first two-mode cavity can introduce a phase to the logical state  $|a 10\rangle$  when the

atom is detuned from the first mode  $\hat{n}_1$  of a qubit, and far detuned from the mode  $\hat{n}_2$ . Then, another atom in  $|a\rangle$  interacting with the second two-mode cavity, where the atom is detuned from  $\hat{n}_4$  and far detuned from  $\hat{n}_3$ , can add a phase to the logic  $|a 01\rangle$ .

## VI. CONCLUSION

A multiphoton resonance can be a very useful technique for applications in quantum information processing as it involves a process conditional on the presence of various photons. Here we use the theory of multiphoton resonance with a multilevel multiphoton Jaynes-Cummings model. Information is stored in photonic qubits and we produce a set of practical one-qubit, two-qubit, and even three-qubit gates. This works because CQED offers a high non-linearity with low losses.

Up to date, the strong interaction between a multilevel atom with a multimode field (such an interaction proposed in our scheme) remains an experimental challenge. In fact, with the remarkable progress in nanotechnology, this kind of interaction might be possible in near future [32]. It is reported in [33] that a transfer of energy between two individual nanoparticles strongly coupled to high-Q whispering-gallery modes in a microsphere resonator is experimentally achieved. This achievement gives a great hope of finding experiments that proceed an interaction between a single multimode cavity interacting with a multilevel atom in the limit of strong coupling.

MMA would like to acknowledge support from King Khalid University (KKU). MSE thanks the Japanese Society for the Promotion of Science. BMG acknowledges the support of the Leverhulme Trust and thanks Michael Hartmann and Bruce W. Shore for comments.

## Appendix A: Adiabatic elimination

Generally, the time evolution of a quantum system is governed by the Schrödinger equation:

$$i \frac{\partial}{\partial t} \mathbf{c}(t) = \mathbf{H} \mathbf{c}(t) \quad (A1)$$

Applying a Laplace transform shows that

$$i(s\bar{\mathbf{c}}(s) - \mathbf{c}(0)) = \mathbf{H} \bar{\mathbf{c}}(s). \quad (A2)$$

An approximate solution in Laplace space, therefore, can be expressed as

$$\bar{\mathbf{c}}(s) = (s\mathbf{I} + i\mathbf{H})^{-1} \mathbf{c}(0). \quad (A3)$$

By assuming that the Hamiltonian  $\mathbf{H}$  to be represented by a  $2 \times 2$  matrix where the states of interest are included in  $\mathbf{W}_0$  and the states eliminated under certain conditions are represented by the matrix  $\mathbf{A}$ ,  $\mathbf{H}$  can be defined as

$$\mathbf{H} = \begin{bmatrix} \mathbf{W}_0 & \mathbf{B} \\ \mathbf{B}^\dagger & \mathbf{A} \end{bmatrix}.$$

Then, the inverse of the square matrix  $(s\mathbf{I} + i\mathbf{H})$  reads

$$(s\mathbf{I} + i\mathbf{H})^{-1} = \begin{bmatrix} -i\mathbf{X}\mathbf{B}(s + i\mathbf{A})^{-1} & \\ -i(s + i\mathbf{A})^{-1}\mathbf{B}^\dagger\mathbf{X} & (s + i\mathbf{A})^{-1} - (s + i\mathbf{A})^{-1}\mathbf{B}^\dagger\mathbf{X}\mathbf{B}(s + i\mathbf{A})^{-1} \end{bmatrix}, \quad (\text{A4})$$

where  $\mathbf{X} = [s + i\mathbf{W}_0 + \mathbf{B}(s + i\mathbf{A})^{-1}\mathbf{B}^\dagger]^{-1}$ .

Equation (A4) can be further simplified by introducing the approximation that the eigenvalues of  $\mathbf{A}$  are much larger in magnitude than the eigenvalues of  $\mathbf{W}_0$  [26]. One then finds that

$$(s\mathbf{I} + i\mathbf{H})^{-1} \sim \begin{bmatrix} [s + i(\mathbf{W}_0 - \mathbf{B}\mathbf{A}^{-1}\mathbf{B}^\dagger)]^{-1} & \mathcal{O}(1/A) \\ \mathcal{O}(1/A) & \mathcal{O}(1/A) \end{bmatrix}$$

The subsystem containing only the states of interest can be, therefore, described by the effective Hamiltonian

$$\mathbf{H}_{\text{eff}} = \mathbf{W}_0 - \mathbf{B}\mathbf{A}^{-1}\mathbf{B}^\dagger.$$

## Appendix B: The iswap Gate

### 1. A two-level approximation

In Sec. III, we have seen that in the interaction picture and with  $|a\ 1010\rangle$  to be the initial state the Hamiltonian of the atom-field system is:

$$H' = \begin{pmatrix} 0 & g_1^{\text{ab}} & 0 & 0 & 0 \\ g_1^{\text{ab}} & \Delta_1 & g_2^{\text{bc}} & 0 & 0 \\ 0 & g_2^{\text{bc}} & \Delta_2 & g_3^{\text{cd}} & 0 \\ 0 & 0 & g_3^{\text{cd}} & \Delta_3 & g_4^{\text{da}} \\ 0 & 0 & 0 & g_4^{\text{da}} & \Delta_4 \end{pmatrix}, \quad (\text{B1})$$

where the system detunings  $\Delta_i$  ( $i = 1, 2, 3, 4$ ) can be defined as

$$\begin{aligned} \Delta_1 &= (\omega_{ba} - \omega_1), \\ \Delta_2 &= (\omega_{ba} - \omega_1) - (\omega_{bc} - \omega_2), \\ \Delta_3 &= (\omega_{ba} - \omega_1) - (\omega_{bc} - \omega_2) + (\omega_{dc} - \omega_3), \\ \Delta_4 &= (\omega_{ba} - \omega_1) - (\omega_{bc} - \omega_2) + (\omega_{dc} - \omega_3) - (\omega_{da} - \omega_4). \end{aligned} \quad (\text{B2})$$

By following Shore's method above, the basis states given by  $|\Psi(t)\rangle$  in Eq. (12) can be divided into a couple of subsystems  $\mathbb{P}|\Psi(t)\rangle$  and  $\mathbb{Q}|\Psi(t)\rangle$ , where  $\mathbb{P}$  and  $\mathbb{Q}$  are orthogonal projection operators and  $\mathbb{P} + \mathbb{Q} = 1$ . Assuming  $\mathbb{P}$  consists of the states  $|a10\rangle$  and  $|a01\rangle$ , one finds that the operators  $H_0 = \mathbb{P}H\mathbb{P}$ ,  $A = \mathbb{Q}H\mathbb{Q}$ , and  $B = \mathbb{P}H\mathbb{Q}$  can be expressed, in the matrix formalism, as

$$\begin{aligned} H_0 &= \begin{bmatrix} 0 & 0 \\ 0 & \Delta_4 \end{bmatrix}, \quad B = \begin{bmatrix} g_1^{\text{ab}} & 0 & 0 \\ 0 & 0 & g_4^{\text{ad}} \end{bmatrix}, \\ A &= \begin{bmatrix} \Delta_1 & g_2^{\text{bc}} & 0 \\ g_2^{\text{bc}} & \Delta_2 & g_3^{\text{cd}} \\ 0 & g_3^{\text{cd}} & \Delta_3 \end{bmatrix}. \end{aligned} \quad (\text{B3})$$

An effective two-level Hamiltonian  $H_{\text{eff}}$  can be constructed by  $H_{\text{eff}} = H_0 - B A^{-1} B^\dagger$ . The effective coupling

is found to be

$$\begin{aligned} g_{\text{eff}} &= -\frac{g_1^{\text{ab}} g_2^{\text{bc}} g_3^{\text{cd}} g_4^{\text{da}}}{\Delta_1 \Delta_2 \Delta_3 - \Delta_3 (g_2^{\text{bc}})^2 - \Delta_1 (g_3^{\text{cd}})^2}, \\ &\approx -\frac{g_1^{\text{ab}} g_2^{\text{bc}} g_3^{\text{cd}} g_4^{\text{da}}}{\Delta_1 \Delta_2 \Delta_3}, \end{aligned} \quad (\text{B4})$$

and the effective detuning of the two-level system is

$$\begin{aligned} \Delta_{\text{eff}} &= \\ \Delta_4 &+ \frac{(g_1^{\text{ab}})^2 (\Delta_2 \Delta_3 - (g_3^{\text{cd}})^2) - (g_4^{\text{da}})^2 (\Delta_1 \Delta_2 - (g_2^{\text{bc}})^2)}{\Delta_1 \Delta_2 \Delta_3 - \Delta_3 (g_2^{\text{bc}})^2 - \Delta_1 (g_3^{\text{cd}})^2}, \\ &\approx \Delta_4 + \frac{(g_1^{\text{ab}})^2}{\Delta_1} - \frac{(g_4^{\text{da}})^2}{\Delta_3}. \end{aligned} \quad (\text{B5})$$

### 2. A three-level system

In the case of  $\mathbb{Q} = |c, 0110\rangle\langle c, 0110| + |d, 0100\rangle\langle d, 0100|$ , the operators  $H_0$ ,  $B$ , and  $A$  can be given as

$$\begin{aligned} H_0 &= \begin{bmatrix} 0 & g_1^{\text{ab}} & 0 \\ g_1^{\text{ab}} & \Delta_1 & 0 \\ 0 & 0 & \Delta_4 \end{bmatrix}, \quad B = \begin{bmatrix} 0 & 0 \\ g_2^{\text{bc}} & 0 \\ 0 & g_4^{\text{da}} \end{bmatrix}, \\ A &= \begin{bmatrix} \Delta_2 & g_3^{\text{cd}} \\ g_3^{\text{cd}} & \Delta_3 \end{bmatrix}. \end{aligned} \quad (\text{B6})$$

In the space  $\{|a1010\rangle, |b0010\rangle, |a0101\rangle\}$ , the effective Hamiltonian  $H_{\text{eff}}$  can be constructed as

$$H_{\text{eff}} = \begin{bmatrix} 0 & g_{(1)}^{\text{eff}} & 0 \\ g_{(1)}^{\text{eff}} & \Delta_1^{\text{eff}} & g_{(2)}^{\text{eff}} \\ 0 & g_{(2)}^{\text{eff}} & \Delta_2^{\text{eff}} \end{bmatrix}, \quad (\text{B7})$$

and then the corresponding effective couplings and detunings can be expressed as

$$g_{\text{eff}}^{(1)} = g_1^{\text{ab}}, \quad g_{\text{eff}}^{(2)} = \frac{g_2^{\text{bc}} g_3^{\text{cd}} g_4^{\text{da}}}{(\Delta_2 \Delta_3 - (g_3^{\text{cd}})^2)} \approx \frac{g_2^{\text{bc}} g_3^{\text{cd}} g_4^{\text{da}}}{\Delta_2 \Delta_3} \quad (\text{B8})$$

and the effective detunings

$$\begin{aligned} \Delta_{\text{eff}}^{(1)} &= \Delta_1 - \frac{(g_2^{\text{bc}})^2 \Delta_3}{(\Delta_2 \Delta_3 - (g_3^{\text{cd}})^2)} \approx \Delta_1 - \frac{(g_2^{\text{bc}})^2}{\Delta_2}, \\ \Delta_{\text{eff}}^{(2)} &= \Delta_4 - \frac{(g_4^{\text{da}})^2 \Delta_2}{(\Delta_2 \Delta_3 - (g_3^{\text{cd}})^2)} \approx \Delta_4 - \frac{(g_4^{\text{da}})^2}{\Delta_3}. \end{aligned} \quad (\text{B9})$$

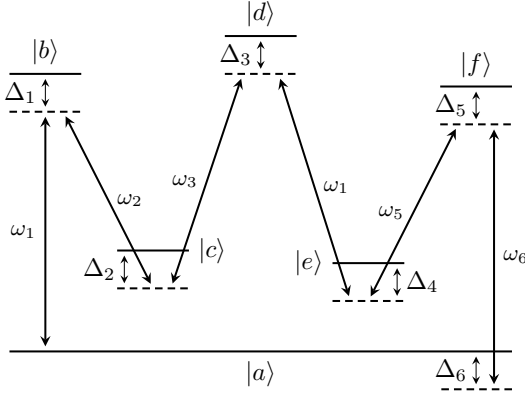


FIG. 15. Energy level scheme for a Fredkin gate. Note the repeated mode  $\omega_1$ . Operation requires at least  $\Delta_6 \sim 0$ .

### Appendix C: A Fast Fredkin Gate

The Fredkin gate, as a three-qubit gate, can be realized in our scheme as mentioned in Sec. V. Considering Fig. 15, this system is governed by the Hamiltonian  $H$

$$H = \sum_i \omega_i \sigma_{ii} + \sum_j \omega_j a_j^\dagger a_j + [g_1 \sigma_{ba} a_1 + g_2 \sigma_{cb} a_2^\dagger + g_3 \sigma_{dc} a_3 + g_1 \sigma_{ed} a_1^\dagger + g_5 \sigma_{fe} a_5 + g_6 \sigma_{af} a_6^\dagger + \text{H.c.}] , \quad (\text{C1})$$

where  $(i = a, b, c, d, e, f)$  and  $(j = 1, 2, 3, 5, 6)$ . Beginning with the initial state of the atom-field system  $|\Psi(0)\rangle = |a\ 10, 01, 10\rangle \equiv |a\ 101\rangle$ , the time evolution of  $|\Psi(0)\rangle$  can be a superposition

$$|\Psi(t)\rangle = c_1(t) |a\ 10, 01, 10\rangle + c_2(t) |b\ 00, 01, 10\rangle + c_3(t) |c\ 00, 11, 10\rangle + c_4(t) |d\ 00, 10, 10\rangle + c_5(t) |e\ 10, 10, 10\rangle + c_6(t) |f\ 10, 10, 00\rangle + c_7(t) |a\ 10, 10, 01\rangle + c_8(t) |b\ 00, 10, 01\rangle + c_9(t) |c\ 00, 20, 01\rangle . \quad (\text{C2})$$

As shown above, the system does not terminate in the atomic state  $|a\rangle$ , and this system has the over-shot states  $|b\ 00, 10, 01\rangle$  and  $|c\ 00, 20, 01\rangle$ . To avoid these states to be populated, we always assume the detunings  $\Delta_1$  and  $\Delta_2$  to be very large. The definitions of the detunings in Eq. (B2) can be easily employed to define the system detunings  $\Delta_i$  (with  $i = 1, 2, \dots, 6$ ) in the Fredkin gate.

An effective three-level behaviour can be analysed by allowing the  $\mathbb{P}$ -space to include  $|a, 101\rangle$ ,  $|d\rangle$ , and  $|a, 110\rangle$ . The states  $|b, 00, 01, 10\rangle$ ,  $|c, 00, 11, 10\rangle$ ,  $|e, 10, 10, 10\rangle$ ,  $|f, 10, 10, 00\rangle$ ,  $|b, 00, 10, 01\rangle$ , and  $|c, 00, 20, 01\rangle$  must be off-resonant so that they remain unpopulated. The required operators for the effective Hamiltonian  $H_{\text{eff}} = H_0 - BA^{-1}B^\dagger$  can be expressed as

$$H_0 = \begin{bmatrix} 0 & 0 & 0 \\ 0 & \Delta_3 & 0 \\ 0 & 0 & \Delta_6 \end{bmatrix}, \quad B = \begin{bmatrix} g_1^{\text{ab}} & 0 & 0 & 0 & 0 & 0 \\ 0 & g_3^{\text{cd}} & g_1^{\text{de}} & 0 & 0 & 0 \\ 0 & 0 & 0 & g_6^{\text{af}} & g_1^{\text{ab}} & 0 \end{bmatrix},$$

$$A = \begin{bmatrix} \Delta_1 & g_2^{\text{bc}} & 0 & 0 & 0 & 0 \\ g_2^{\text{bc}} & \Delta_2 & 0 & 0 & 0 & 0 \\ 0 & 0 & \Delta_4 & g_5^{\text{ef}} & 0 & 0 \\ 0 & 0 & g_5^{\text{ef}} & \Delta_5 & 0 & 0 \\ 0 & 0 & 0 & 0 & \Delta_6 + \Delta_1 & g_2^{\text{bc}}\sqrt{2} \\ 0 & 0 & 0 & 0 & g_2^{\text{bc}}\sqrt{2} & \Delta_6 + \Delta_2 \end{bmatrix}. \quad (\text{C3})$$

Within states  $|10, 01, 10, a\rangle$ ,  $|00, 10, 10, d\rangle$  and  $|10, 10, 01, a\rangle$ , the effective Hamiltonian  $H_{\text{eff}}$  can be given by Eq. (B7) where

$$g_{(1)}^{\text{eff}} = \frac{g_1^{\text{ab}} g_2^{\text{bc}} g_3^{\text{cd}}}{\Delta_1 \Delta_2}, \quad g_{(2)}^{\text{eff}} = \frac{g_1^{\text{de}} g_5^{\text{ef}} g_6^{\text{fa}}}{\Delta_4 \Delta_5},$$

and

$$\Delta_1^{\text{eff}} \approx \Delta_3 + \frac{(g_1^{\text{ab}})^2}{\Delta_1} - \frac{(g_3^{\text{cd}})^2}{\Delta_2} - \frac{(g_1^{\text{de}})^2}{\Delta_4},$$

$$\Delta_2^{\text{eff}} \approx \Delta_6 - \frac{(g_6^{\text{af}})^2}{\Delta_5}.$$

### Appendix D: The not gate

The realisation of the single-qubit NOT gate is possible in our scheme. Considering the model in Fig. 14, we assume a de-excited three-level atom in the  $\Lambda$  configuration interacts with a dual-rail photonic qubit  $|10\rangle$  or  $|01\rangle$ . The initial state, therefore, can be either the logic  $|a\ 10\rangle$  or  $|a\ 01\rangle$ . Then, the atom interacts with a classical field on the transition  $|c\rangle \mapsto |a\rangle$ . The corresponding Hamiltonian describing all such interactions, i.e. the cavity-atom interaction plus the classical field-atom interaction, can be defined as

$$H = \omega_a \sigma_{aa} + \omega_b \sigma_{bb} + \omega_c \sigma_{cc} + \omega_1 a_1^\dagger a_1 + \omega_2 a_2^\dagger a_2 + \left[ g_1^{\text{ab}} a_1^\dagger \sigma_{ab} + g_2^{\text{bc}} \sigma_{bc} a_2 + (\Omega/2) e^{i\omega_3 t} \sigma_{ac} + \text{H.C.} \right]. \quad (\text{D1})$$

Given the system in the initial state  $|\Psi(0)\rangle = |a\ 10\rangle$ , this state evolves into a superposition

$$|\Psi(t)\rangle = c_{c10}(t) |c\ 10\rangle + c_{a10}(t) |a\ 10\rangle + c_{b00}(t) |b\ 00\rangle + c_{c01}(t) |c\ 01\rangle + c_{a01}(t) |a\ 01\rangle . \quad (\text{D2})$$

Then, by using the Schrödinger equation  $\frac{\partial}{\partial t} |\Psi(t)\rangle = -iH |\Psi(t)\rangle$  a set of amplitude equations, within the rotating wave approximation, can be obtained. To transform these amplitude equations to the frame rotating with the frequencies of the optical fields  $\omega_1$ ,  $\omega_2$ , and  $\omega_{\text{class}}$ , we introduce the transformation (note that the initial state

$|a\ 10\rangle$  is set as a zero point energy)

$$\begin{aligned}
c_{c10}(t) &= c'_{c10}(t) e^{-i(\omega_a + \omega_{\text{class}})t} e^{-i\omega_1 t}, \\
c_{a10}(t) &= c'_{a10}(t) e^{-i\omega_a t} e^{-i\omega_1 t}, \\
c_{b00}(t) &= c'_{b00}(t) e^{-i(\omega_a + \omega_1)t}, \\
c_{c01}(t) &= c'_{c01}(t) e^{-i(\omega_a + \omega_1 - \omega_2)t} e^{-i\omega_2 t}, \\
c_{a01}(t) &= c'_{a01}(t) e^{-i(\omega_a + \omega_1 - \omega_2 - \omega_{\text{class}})t} e^{-i\omega_2 t}.
\end{aligned} \tag{D3}$$

The RWA Hamiltonian, then, can be re-expressed as

$$H' = \begin{bmatrix} (\Delta_2 - \Delta_3) & \Omega/2 & 0 & 0 & 0 \\ \Omega/2 & 0 & g_1^{\text{ab}} & 0 & 0 \\ 0 & g_1^{\text{ab}} & \Delta_1 & g_2^{\text{bc}} & 0 \\ 0 & 0 & g_2^{\text{bc}} & \Delta_2 & \Omega/2 \\ 0 & 0 & 0 & \Omega/2 & \Delta_3 \end{bmatrix}, \tag{D4}$$

where  $H'$  acts in the basis  $\{|c\ 10\rangle, |a\ 10\rangle, |b\ 00\rangle, |c\ 01\rangle, |a\ 01\rangle\}$ . Now the basis states other than  $|a\ 10\rangle$  and  $|a\ 01\rangle$  can be adiabatically eliminated by recalling Shore's method. That is, we allow large values for  $\Delta_1, \Delta_2$ . In other words, we assume the states  $|a\ 10\rangle$  and  $|a\ 01\rangle$  to be spanned by the space  $\mathbb{P}$  and the remaining states to be set in the space

of  $\mathbb{Q}$ . The resultant operators, then, can be given as

$$\begin{aligned}
H_0 &= \begin{bmatrix} 0 & 0 \\ 0 & \Delta_3 \end{bmatrix}; B = \begin{bmatrix} \Omega/2 & g_1^{\text{ab}} & 0 \\ 0 & 0 & \Omega/2 \end{bmatrix}; \\
A &= \begin{bmatrix} (\Delta_2 - \Delta_3) & 0 & 0 \\ 0 & \Delta_1 & g_2^{\text{bc}} \\ 0 & g_2^{\text{bc}} & \Delta_2 \end{bmatrix}. \tag{D5}
\end{aligned}$$

The corresponding effective detuning with  $\Delta_{1,2} \gg g_{1,2}, \Omega/2, \Delta_3$  is

$$\begin{aligned}
H_{\text{eff}} &= \Delta_3 - \frac{(\Omega/2)^2 \Delta_1}{(\Delta_1 \Delta_2 - (g_2^{\text{bc}})^2)} + \frac{(\Omega/2)^2}{(\Delta_2 - \Delta_3)} \\
&\quad + \frac{(g_1^{\text{ab}})^2 \Delta_1}{(\Delta_1 \Delta_2 - (g_2^{\text{bc}})^2)} \\
&\approx \Delta_3 + \frac{(g_1^{\text{ab}})^2}{\Delta_2}, \tag{D6}
\end{aligned}$$

and the effective coupling strength is

$$g_{\text{eff}} = \frac{(\Omega/2) g_1^{\text{ab}} g_2^{\text{bc}}}{(\Delta_1 \Delta_2 - (g_2^{\text{bc}})^2)} \approx \frac{\Omega g_1^{\text{ab}} g_2^{\text{bc}}}{2\Delta_1 \Delta_2}. \tag{D7}$$

At the resonance condition, the time evolution of the initial state  $|a\ 10\rangle$  or  $|a\ 01\rangle$  can be given by Eq. (16), and with an appropriate interaction time  $g_{\text{eff}} t_{\text{int}}$  and a global phase the Pauli  $X$  gate can be easily realized, and the exponential of the NOT gate is nothing but the rotation operator  $R_x(g_{\text{eff}} t)$ .

- 
- [1] B. Lounis and W. E. Moerner, *Nature* **407**, 491 (2000).
  - [2] C. Santori, M. Pelton, G. Solomon, Y. Dale, and Y. Yamamoto, *Phys. Rev. Lett.* **86**, 1502 (2001).
  - [3] K. Matthias, L. Birgit, H. Kazuhiro, L. Wolfgang, and W. Herbert, *Nature* **431**, 1075 (2004).
  - [4] N. Imoto, H. A. Haus, and Y. Yamamoto, *Phys. Rev. A* **32**, 2287 (1985).
  - [5] I. L. Chuang and Y. Yamamoto, *Phys. Rev. A* **52**, 3489 (1995).
  - [6] H. Schmidt and A. Imamoglu, *Opt. Lett.* **21**, 1936 (1996).
  - [7] P. Kok, H. Lee, and J. P. Dowling, *Phys. Rev. A* **66**, 063814 (2002).
  - [8] P. Kok, W. J. Munro, K. Nemoto, T. C. Ralph, J. P. Dowling, and G. J. Milburn, *Rev. Mod. Phys.* **79**, 135 (2007).
  - [9] E. Knill, R. Laflamme, and G. J. Milburn, *Nature* **409**, 46 (2001).
  - [10] T. Rudolph and J.-W. Pan, arXiv:quant-ph/0108056 (2001).
  - [11] E. Jaynes and F. Cummings, *Proc. IEEE* **51**, 89 (1963).
  - [12] J. Larson and B. M. Garraway, *J. Mod. Opt.* **51**, 1691 (2004).
  - [13] C. C. Gerry and J. H. Eberly, *Phys. Rev. A* **42**, 6805 (1990).
  - [14] M. S. Everitt and B. M. Garraway, arXiv:1407.0239 (2014).
  - [15] I. L. Chuang and Y. Yamamoto, *Phys. Rev. Lett.* **76**, 4281 (1996).
  - [16] R. J. Cook and B. W. Shore, *Phys. Rev. A* **20**, 539 (1979).
  - [17] N. Schuch and J. Siewert, *Phys. Rev. A* **67**, 032301 (2003).
  - [18] T. Tanamoto, Y.-X. Liu, X. Hu, and F. Nori, *Phys. Rev. Lett.* **102**, 100501 (2009).
  - [19] R. Raussendorf and H. J. Briegel, *Phys. Rev. Lett.* **86**, 5188 (2001).
  - [20] R. Raussendorf, D. E. Browne, and H. J. Briegel, *Phys. Rev. A* **68**, 022312 (2003).
  - [21] R. J. Cook and B. W. Shore, *Phys. Rev. A* **20**, 539 (1979).
  - [22] G. Lindblad, *Communications in Mathematical Physics* **48**, 119 (1976).
  - [23] J. Dalibard, Y. Castin, and K. Mølmer, *Phys. Rev. Lett.* **68**, 580 (1992).
  - [24] K. Mølmer, Y. Castin, and J. Dalibard, *JOSA B* **10**, 524 (1993).
  - [25] R. Dum, P. Zoller, and H. Ritsch, *Phys. Rev. A* **45**, 4879 (1992).
  - [26] B. W. Shore, *Phys. Rev. A* **24**, 1413 (1981).
  - [27] S. Kuhr, S. Gleyzes, C. Guerlin, J. Bernu, U. B. Hoff, S. Deléglise, S. Osnaghi, M. Brune, J.-M. Raimond, S. Haroche, E. Jacques, P. Bosland, and B. Visentin, *Appl. Phys. Lett.* **90**, 164101 (2007).
  - [28] E. Fredkin and T. Toffoli, *International Journal of Theoretical Physics* **21**, 219 (1982).
  - [29] M. A. Nielsen and I. L. Chuang, *Quantum computation and quantum information*. (Cambridge University Press, Cambridge, 2000).



- [30] S. M. Barnett, *Quantum information* (Oxford University Press, 2009).
- [31] B. Englert, M. Löffler, O. Benson, B. Varcoe, M. Weidinger, and H. Walther, *Fortschr. Phys.* **46**, 897 (1998).
- [32] J. T. Chang and M. S. Zubairy, *Phys. Rev. A* **77**, 012329 (2008).
- [33] S. Götzinger, L. d. S. Menezes, A. Mazzei, S. Kühn, V. Sandoghdar, and O. Benson, *Nano Lett.* **6**, 11511154 (2006).